International Journal of Thermophysics, Vol. 26, No. 4, July 2005 (© 2005)
DOI: 10.1007/s10765-005-6707-7

Electrical Resistivity and Thermodynamic Properties of Dense Tungsten Plasma[1]

A. W. DeSilva[2] and A. D. Rakhel[3,4]

Tungsten wires immersed in a water bath were rapidly heated by a pulse current. The electrical resistivity as a function of the plasma density, which varied as the plasma column expanded, and as a function of internal energy was measured. In order to specify the parameters of the experiments to approach homogeneity of the physical quantities across the column, one-dimensional (1D) magneto-hydrodynamic (MHD) simulations of the pulse Joule heating dynamics were conducted. As a result, the resistivity of dense tungsten plasma along with the complete set of thermodynamic quantities (pressure, density, and internal energy) were directly measured without using any equation of state (EOS) model of tungsten. Present results indicate that the dependence of the resistivity of tungsten on internal energy along isochors is flat at high densities, but acquires a strong negative slope at a density which is 8–16 times lower than the normal solid density when the internal energy is in a range of 5–14 $kJ \cdot g^{-1}$.

KEY WORDS: dense metal plasma; electrical resistivity; exploding wire technique; metal–nonmetal transition; MHD simulations; tungsten.

1. INTRODUCTION

Dense metal plasma characterized by strong inter-particle interactions (strongly coupled plasma) is a very interesting subject because it provides insight into the physics of the metal–nonmetal transition, plasma phase

[1] Paper presented at the Seventh International Workshop on Subsecond Thermophysics, October 6–8, 2004, Orléans, France.

[2] Institute for Research in Electronics and Applied Physics, University of Maryland, College Park, Maryland 20742, U.S.A.

[3] Institute for High Energy Densities, Izhorskaya 13/19, Moscow 125412, Russia.

[4] To whom correspondence should be addressed. E-mail: rakhel@rakhel.msk.ru

transitions, etc. [1]. Measurements of thermodynamic and transport properties of such plasmas are benchmarks for theories and computer simulations relevant to the study of dense stars (dwarfs) and planetary interiors (Jovian planets). There is also practical interest in connection with some laboratory applications. For instance, to increase the efficiency of the wire-array Z-pinches, as intense sources of X-rays for the inertial confinement fusion application [2], thermodynamic and transport properties of tungsten should be known in wide domains of density and temperature (including the condensed and gaseous states) to perform simulation of the Z-pinch dynamics.

At present, experimental information on the electrical resistivity and thermodynamic properties of dense tungsten plasma is very limited [3–5]. The published experimental data [3, 5] are not comprehensive, as the measured quantities do not characterize completely the thermodynamic state of the plasmas generated in those experiments; different semi-empirical equation-of-state (EOS) models were used to obtain the missing quantities. In addition, the accuracy of the data presented in Refs. 3 and 4 is questionable because of the plasma inhomogeneity.

In the present work we report measured results on the electrical resistivity of dense tungsten plasma along with a complete set of thermodynamic quantities (pressure, density, and internal energy) without using any EOS model of tungsten. Special attention is paid to ensure a homogeneous state in the plasma generated during the measurements. Our results demonstrate the dependence of the resistivity of tungsten on the internal energy and density when it passes from the condensed into a gaseous state.

2. EXPERIMENT

The technique used here is the rapid Joule heating of thin metal wires in a water bath [3]. The water serves as a damper, resisting the free expansion of the plasma column formed by the wire and forcing the column to remain approximately uniform during the expansion (when the heating conditions are chosen properly). Diagnostics are the current and voltage measurements and the streak images of the expanding plasma column. The current is measured with a Rogowsky loop and then is passively integrated with an RC integrating circuit, with subsequent correction for the RC time constant made in the numerical analysis. The precision of the current measurement is estimated to be 3–4%. The voltage is measured with a low inductance oil-filled divider (with a precision of about 3–5%). The current and voltage signals of different experiments with all parameters constant show a scatter of less than 9%. Tungsten wire samples (supplied by Goodfellow Metals, 99.95% purity by mass) with diameters of

$125 \pm 1\,\mu m$ and $250 \pm 1\,\mu m$ have been used in this work. Samples are 26.7 ± 1 mm in length, and are attached with low resistance clamps at the ends to the electrodes delivering the heating current. Pulse heating of the samples is accomplished by discharging a $3.76\,\mu F$ capacitor bank which is switched by a triggered spark-gap. The discharge circuit used of 30 nH short-circuit inductance, depending on the applied voltage (from 9 to 25 ± 1 kV), generates a pulse current rising in 2–0.2 μs to its maximum value. The temporal dependences of the current through a 250-μm wire, the resistive part of the voltage drop across its length, and the specific Joule heat imparted into the wire are shown in Fig. 1.

To obtain a streak image of the expanding plasma column formed by the wire, it is back-lighted by a xenon flash lamp and imaged on a slit oriented perpendicular to the wire axis. A rotating mirror sweeps the light passing through the slit onto the input of an ICCD camera (Stanford Computer Optics 4-Quik-E 50-18). Two wires of 25-μm diameter across the slit produce a pair of black lines on the streak image establishing a spatial scale, and a pair of triggered sparks at the slit produce two spots on the image that allow the writing speed to be determined accurately (See Fig. 2). The current through the sparks is recorded and used to relate a diameter-time temporal dependence obtained from the streak image with those of the electrical quantities. The plasma column diameter is determined with a precision of 4–7%. All electrical waveforms are recorded

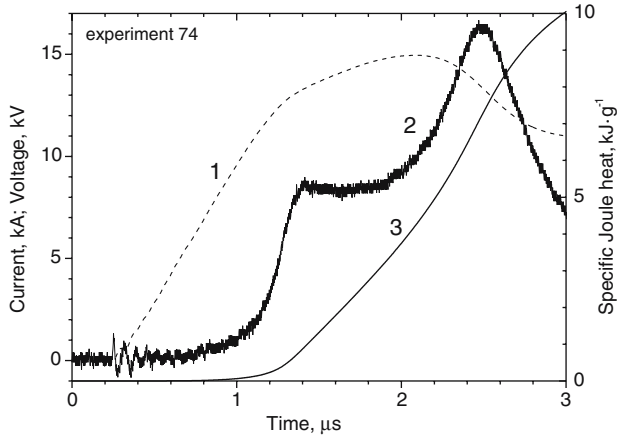

Fig. 1. Temporal dependences of (1) the current through the wire, (2) the resistive part of the voltage drop across its length, and (3) the specific Joule heat imparted into it. Pulse heating was accomplished by discharging through a 250 μm tungsten wire the capacitor bank charged to an initial voltage of about 15 kV.

using two 2-channel, 1-GHz digital scopes (HP model 54111D). In Fig. 2 a complement streak image of the plasma column is shown for the experiment for which electrical quantities are presented in Fig. 1.

To estimate the uncertainty of our current and voltage measurements and to verify that the resistive portion of the sample voltage drop is determined correctly, we compared the normalized resistance R^* of the wire as a function of the specific Joule heat released in it with reliable literature data. We normalize the resistance R by multiplying it by the ratio of the initial cross-sectional area of the wire S_0 to the length l;

$$R^* = RS_0/l, \tag{1}$$

In other words, R^* is the resistivity calculated assuming the initial sample dimensions. For the case of homogeneous heating, R^* is expressed through the resistivity σ^{-1}(σ is the electrical conductivity) and the relative specific volume of the wire material V/V_0 by

$$R^* = \sigma^{-1}\frac{V_0}{V} \tag{2}$$

In the next section it will be shown that the dynamic pressure generated in our experiments is within 2–5 kbar when the sample resides in

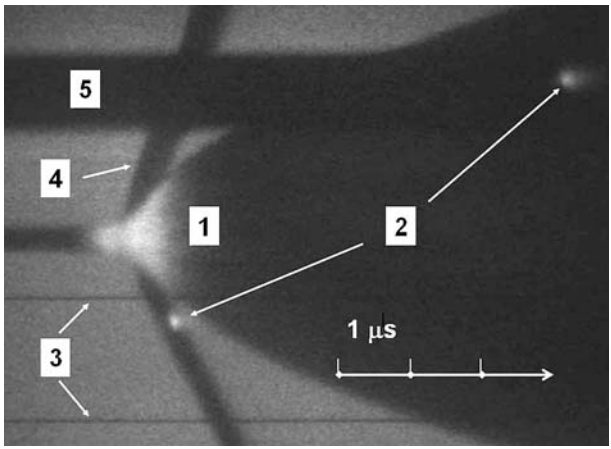

Fig. 2. Complement streak image of the plasma column formed for the experiment of which electrical quantities are presented in Fig. 1 (1), two spots produced by a pair of triggered sparks (2) give time marks, two wires of 25 μm diameter across the slit (3) establish a spatial scale, and a shock wave in the surrounding water (4). Black streak (5) is due to a light block preventing the second spark light to be washed out by the plasma light.

the condensed state region. These pressures are very close to those at which the measurements of Refs. 6 and 7 were carried out (2–4 kbar). The dependences of the normalized resistance versus the specific Joule heat for three experiments performed in this study and those from Refs. 6, 7, and 8 are plotted in Fig. 3. As one can see, our measurements are consistent within the stated error limit with literature data.

3. HOMOGENEOUS HEATING

To obtain the electrical resistivity and other specific quantities (specific internal energy and density) from the measured quantities (current, voltage, and the plasma column diameter), the plasma column with sufficiently uniform radial distributions of the temperature and density should be generated in the experiment. In order to approach homogeneous heating, the parameters of the experiments were found using one-dimensional magneto-hydrodynamic (1D MHD) simulations. To describe the hydrodynamic flow generated in the wire material and surrounding water when an electrical current pulse is applied to the wire, the 1D MHD model developed in Refs. 5, 8, and 9 was utilized. The corresponding set of equations of the model consists of the local laws of conservation of mass, linear momentum, and energy together with Maxwell's equations and the equations for the discharge circuit producing the current pulse. The 1D approximation implies that all physical quantities in the model are functions of

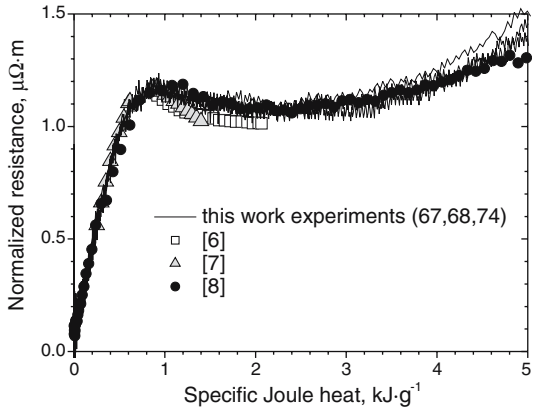

Fig. 3. Comparisons of the normalized resistance as a function of the specific Joule heat imparted into the wire for three experiments (with 125 and 250 μm tungsten wires) to literature data.

only the radius vector r and the time t. It is easy to see that effects of the heat conduction, viscosity, and radiation may be neglected under these conditions so that they were ignored in the simulations. Evaporation from the wire surface can be neglected also, since this process is governed by the heat conduction transport from the bulk to the wire surface. Only the volume vaporization (boiling) was taken into account in the simulations. The hydrodynamic flow was computed for two regions: the wire and surrounding water assuming that the substances do not mix with each other at the boundary. Thermodynamic functions of tungsten and the electrical resistivity model used in these simulations are described in Refs. 8 and 9.

For the hydrodynamic calculations we need also an EOS model of water. The following semi-empirical EOS describing adiabatic flow generated in water was utilized:

$$P = \frac{B}{n}\left[\left(\frac{\rho}{\rho_{O_2}}\right)^n - 1\right] \tag{3}$$

where the coefficient B and the exponent n are assumed to be constant. These constants are related by an equation with the sound speed and density ρ_{0_2} of water at standard conditions. The coefficients B and n were found by fitting of the data from Refs. 10 and 11 ($B = 2.25$ GPa and $n = 7.0$).

The simulation results of the pulse Joule heating dynamics of the tungsten wires submersed in water have shown that for some parameters of the experiments a sufficiently homogeneous plasma column can be created. The parameters which were varied in the simulations to meet the homogeneous heating conditions were the following: the wire diameter and its length, the initial voltage at the capacitor bank, and the discharge circuit parameters (additional resistance and inductance in series with the wire). The path in the P, T plane of sufficiently homogeneous heating predicted by the simulations and realized in our subsequent experiments is presented in Fig. 4. Such heating is predicted for a 125 μm diameter tungsten wire of 26.75 mm in length, when the discharge circuit inductance is 1100 nH and the initial voltage at the capacitor bank is 25 kV. The thermodynamic state of the wire is illustrated by five trajectories representing five thin layers (cylindrical shells corresponding to five cells of a spatial mesh for Lagrangian coordinate having in total 60 cells in the wire region): a surface layer (periphery), a layer near the axis of the wire (axis), and three layers between them. To relate the paths to the temporal dependences, the time marks are indicated. As follows from Fig. 4, variations of the temperature across the plasma column do not exceed about 15%. The pressure variations are remarkably larger, especially in the condensed state, but at lower densities they decrease to about 20%.

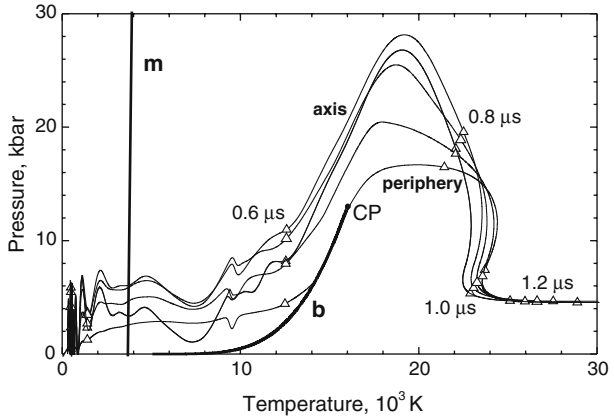

Fig. 4. Evolution of the thermodynamic state of a 125 μm tungsten wire placed in water during pulse Joule heating calculated by means of 1D MHD code. Thermodynamic paths of five fixed particles of the sample (in the sense of the continuous media mechanics) are presented: a particle situated close to the specimen surface (periphery), a particle near the axis (axis), and three particles between them. Also are shown the melting line (m) [12], and the boiling curve (b) with a critical point (CP) calculated by means of the EOS model developed in Refs. 8 and 9. Open triangles indicate the time marks in 0.2 μs interval starting from the moment when the current is switched on.

Radial density profiles across the column at three times for such heating are shown in Fig. 5. The density profiles in the surrounding water are presented also to show the shock wave generated in water.

The simulations have shown that there are essentially two factors preventing an increase of the radial inhomogeneity. The first is the sufficiently high pressure generated in the wire which causes the thermodynamic paths to go above the liquid-vapor boundary preventing vaporization in the bulk of the wire. Therefore, in this case the inertia effects in the two-phase liquid–gas mixture leading to strongly nonuniform radial distributions of the physical quantities across the column [8] are absent. The second factor improving the homogeneity is a proper temporal dependence of the Joule heating power realized for the chosen set of parameters of the heating process. For such heating the radial distributions developed at the early times ($t < 0.75\,\mu s$) are reversed so that the maxima in the temperature and pressure profiles move from the near axis region to the periphery (see Fig. 4).

The degree of radial nonuniformity of the basic quantities can be represented by the standard deviations of the quantities from their mean

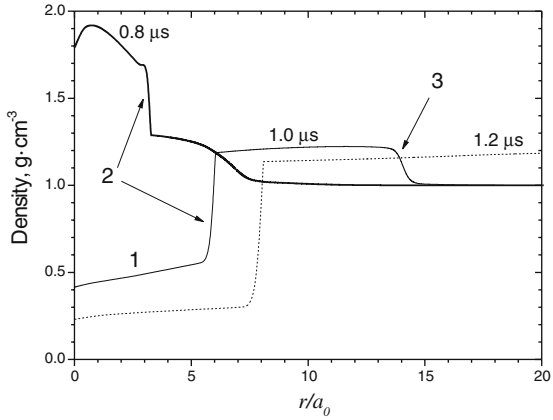

Fig. 5. Three density profiles in the plasma column and surrounding water for the heating process presented in Fig. 4: (1) the plasma column region, (2) the plasma–water interface, and (3) the shock wave. Here a_0 is the initial radius of the wire (125 μm).

values. The mean value of a quantity x across the column is defined as

$$\bar{x} = \int_0^{a(t)} x\rho(r,t)rdr \Big/ \int_0^{a(t)} \rho(r,t)rdr \tag{4}$$

where $\rho(r,t)$ is the density, r is the current radius vector, and $a(t)$ is the column radius. The standard deviations for the specific internal energy, density, and resistivity for the heating process represented in Figs. 4 and 5 are shown in Fig. 6. As one can see the standard deviations of the quantities, and therefore the corresponding uncertainties caused by the radial distributions, do not exceed about 10% at the later times ($t > 0.8\,\mu$s).

4. PROCESSING THE MEASURED DATA

The procedure of processing the primary measured quantities to obtain the resistivity, specific internal energy, density, and pressure was as follows. Using the measured diameter versus time dependence $d(t)$ as an input function with the streak camera, we performed the numerical integration of the 1D hydrodynamic equations of motion in the water region to calculate the pressure at the plasma column boundary (using only the water EOS). Thus, the task about the hydrodynamic flow generated in water by a cylindrical piston moving with a known velocity was solved. Knowing the pressure $P(t)$, we could determine the work performed by

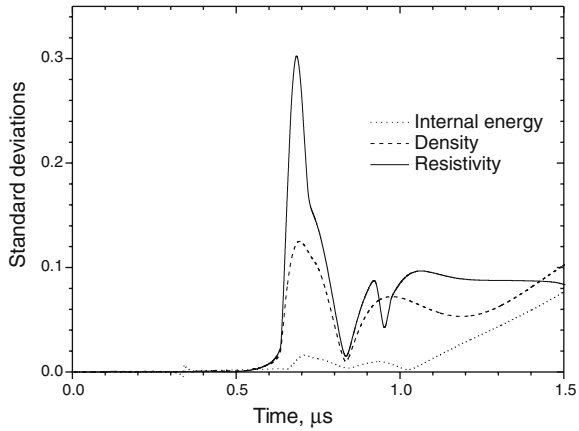

Fig. 6. Standard deviations from the mean values for the calculated quantities corresponding to the basic measured quantities for the heating process presented in Figs. 4 and 5.

the plasma column on the surrounding water and the fraction of the Joule heat imparted into the plasma resulting in its internal energy.

In Fig. 7 the temporal dependences of the plasma column relative radius $a(t)/a_0$ (a_0 is the initial wire radius) and the shock wave trajectory obtained from a streak image are presented. The shock wave trajectory obtained from the 1D hydrodynamic calculation in which the measured dependence $d(t)$ was used as an input function is also shown for comparison. As one can see, there is good agreement between the measured and calculated dependences for the shock wave trajectory. Thus, this figure demonstrates the self-consistency of the pressure and internal energy calculations.[5]

5. RESULTS AND DISCUSSION

The main results of the present study are summarized in Fig. 8 in which the dependences of the resistivity versus specific internal energy are shown for seven of our experiments (thin solid lines with numbers of experiments). The marks (gray) show the resistivity values corresponding to four fixed relative volumes: $V/V_0 = 4$, 8, 16, and 32. Thick solid lines represent least-squares fits of these data. The fitted lines are shown to demonstrate the change in the slope of the dependence of the resistivity on

[5] This comparison proves also that the effect of refraction is negligible in the measurements of the plasma column diameter.

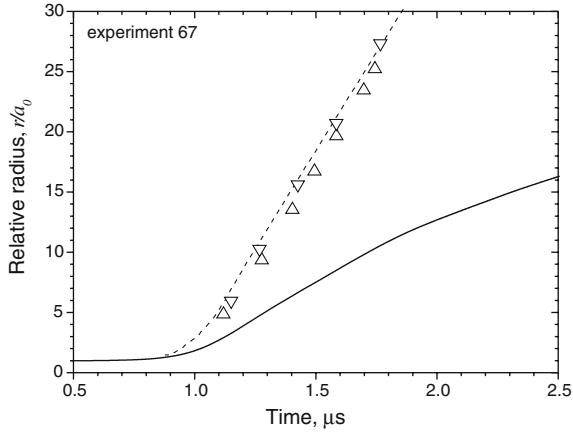

Fig. 7. Temporal dependences of the plasma column relative radius (solid line), the upper edge of the shock wave front position (triangles up) and lower edge of the shock wave front position (triangles down) taken from a streak image of a 125 μm wire, and the shock wave trajectory obtained from 1D hydrodynamic calculation (dashed line) in which the measured dependence of the column radius versus time was used as an input function.

the internal energy along isochors. The correlation coefficients and standard deviations of the fits are presented in Table I. Results of Ref. 5 are shown in this figure with dotted lines. The corresponding values of the resistivity at the four fixed relative volumes are designated with open marks for those data. One value of the resistivity from Ref. 8 (experiment 6, Figs. 1–3 [8]) at $V/V_0 = 4$ is also presented. As can be seen in Fig. 8, our results agree rather well with data from Refs. 5 and 8. It should be noted that in Ref. 5 the resistivity is presented as a function of the relative volume. To compare those data with present results, the dependences for experiments 2, 3, and 11 (Figs. 4 and 5 [5]) were used (See also Figs. 6 and 7 [9]). It should be also noted that the results of Refs. 5 and 9 correspond to substantially higher pressures (30–100 kbar) than those attained in this work.

Present data show that along the isochor $V/V_0 = 4$ the resistivity is practically constant, i.e., there is no dependence on the internal energy and, therefore, on the temperature. A plasma-like dependence of the resistivity on temperature, i.e., a decrease in the resistivity with a rise in temperature is clearly seen for the isochor $V/V_0 = 16$.

Despite a relatively large error in our measurements in the liquid state (mainly due to the uncertainties in the diameter measurements), the

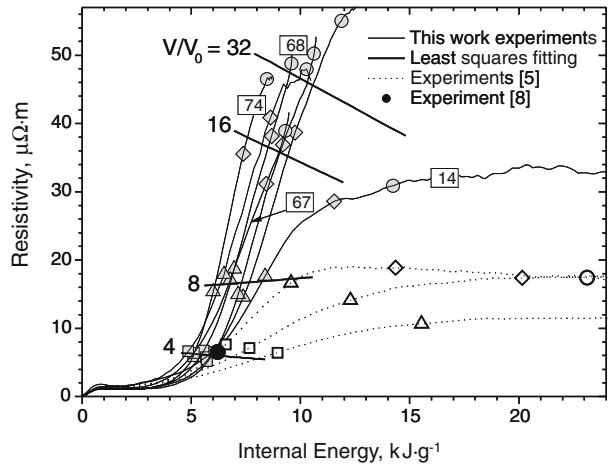

Fig. 8. Electrical resistivity of tungsten versus specific internal energy: experimental data from this work (thin solid lines with the numbers of the experiments), data from this work for four isochors (gray marks), linear fits of data from this work (thick solid lines), results of Ref. 5 for three experiments (dotted lines), resistivity values of Ref. 5 along isochors (corresponding open marks), and one resistivity value from Ref. 8 at $V/V_0 = 4$ (black circle).

Table I. Correlation Coefficients (R) and Standard Deviations (SD) for the Least-Square Fits of the Dependences of the Resistivity versus Internal Energy for Four Isochors Shown in Fig. 8

	$V/V_0 = 4$	$V/V_0 = 8$	$V/V_0 = 16$	$V/V_0 = 32$
R	0.20	0.12	0.45	0.42
SD	0.59	1.8	4.3	8.0

present data show that the resistivity of liquid tungsten depends weakly on internal energy. At an internal energy value of $3\,\mathrm{kJ}\cdot\mathrm{g}^{-1}$ the relative volume of liquid tungsten, according to our measurements, approaches 1.6, which agrees well with an earlier published result [8].

A special effort was made in the present study to estimate the uncertainty of the measurements due to the plasma inhomogeneity. The point is that the simulation of the heating dynamics in the framework of the complete (not dependent on the experiment) 1D MHD model is not very accurate because an EOS and resistivity models are used for which the accuracy is not very high (probably ~30%). To make the computations

of the standard deviations shown in Fig. 6 more relevant to the experiments, they were computed using the measured temporal dependences of the current through the wire and voltage across its length as input functions (since the skin effect for these experiments proved to play practically no role). As a result, it was found that a typical level of uncertainty due to the radial distributions for our experiments presented in Fig. 8 is within 10–30%. The experiment with the highest pressure (experiment 14) has the lowest uncertainty (of about 10%). This experiment shows remarkably lower resistivity values (at a fixed value of the internal energy) compared with those of our other experiments. It should be noted also that the values of the parameters for this experiment (experiment 14) are close to those of the simulations illustrated in Figs. 4–6. Our other experiments have a remarkably higher uncertainty (due to the radial distributions developed in the column) approaching 20–30%. All those experiments show an abrupt increase in the resistivity at an energy value of $5 - 6\,\mathrm{kJ}\cdot\mathrm{g}^{-1}$ and correspond to a lower pressure generated (in comparison to that for experiment 14).

6. CONCLUSION

The electrical resistivity and a complete set of thermodynamic quantities for tungsten have been directly measured in a density range from the normal solid density down to a density 30–40 times lower. It is shown that a plasma-like dependence of the electrical resistivity of expanded tungsten on temperature takes place at a density which is 8–16 times lower than the standard solid density.

REFERENCES

1. V. E. Fortov and I. T. Iakubov, *Physics of Non-ideal Plasmas* (World Scientific Publishing Co. Pte. Ltd., Singapore, New Jersey, London, Hong Kong, 2000).
2. R. B. Spielman, C. Deeney, M. R. Douglas, G. A. Chandler, M. E. Cuneo, T. J. Nash, J. L. Porter, L. E. Ruggles, T. W. L. Sanford, W. A. Stygar, K. W. Struve, M. K. Matzen, D. H. McDaniel, D. L. Peterson, and J. H. Hammer, *Plasma Phys. Control. Fusion* **42**:157 (2000).
3. A. W. DeSilva and J. D. Katsouros, *Int. J. Thermophys.* **20**:1267 (1999).
4. S. Saleem, J. Haun, and H.-J. Kunze, *Phys. Rev. E* **64**:056403 (2001).
5. A. D. Rakhel, V. N. Korobenko, A. I. Savvatimskiy, and V. E. Fortov, *Int. J. Thermophys.* **25**:1203 (2004).
6. U. Seydel, W. Fucke, and H. Wadle, *Die Bestimmung thermophysikalischer Daten flüssiger hochschmelzender Metalle mit schnellen Pulsaufheizexperimenten* (Verlag Dr. Peter Mannhold, Düsseldorf, 1980).
7. A. Berthault, L. Arles, and J. Matricon, *Int. J. Thermophys.* **7**:167 (1986).
8. A. D. Rakhel, A. Kloss, and H. Hess, *Int. J. Thermophys.* **23**:1369 (2002).

9. V. N. Korobenko, A.D. Rakhel, A. I. Savvatimskiy, and V. E. Fortov, *Plasma Physics Reports* **28**:1008 (2002).
10. J. M. Walsh and M. H. Rice. *J. Chem. Phys.* **26**:816 (1957).
11. A. A. Bakanova, V. N. Zubarev, Yu. N. Sutulov, and R.F. Trunin. *Zh. Eksp. Teor. Fiz.* **68**:1099 (1975) [*Sov. Phys. JETP* **41**:544 (1975)].
12. I. S. Grigor'ev and E. Z. Meilikhov, eds., *Physical Quantities (Handbook)* (Energoatomizdat, Moscow, 1991).